Perspective article

A theory of geometry representations for spatial navigation

Taiping Zeng [a,b,c], Bailu Si [d,e,*], Jianfeng Feng [a,b,**]

[a] *Institute of Science and Technology for Brain-Inspired Intelligence, Fudan University, Shanghai, China*
[b] *Key Laboratory of Computational Neuroscience and Brain-Inspired Intelligence (Fudan University), Ministry of Education, China*
[c] *International Research Center for Neurointelligence, Institutes for Advanced Study, University of Tokyo, Tokyo 113-0033, Japan*
[d] *School of Systems Science, Beijing Normal University, Beijing 100875, China*
[e] *Peng Cheng Laboratory, Shenzhen 518055, China*

ARTICLE INFO

ABSTRACT

The geometric information of space, such as environment boundaries, is represented heterogeneously across brain regions. The computational mechanisms of encoding the spatial layout of environments remain to be determined. Here, we postulate a conjunctive encoding theory to illustrate the construct of cognitive maps from geometric perception. The theory naturally describes a spectrum of cell types including experimentally observed boundary vector cells, border cells, "annulus" and "bulls-eye" cells as special examples. In a similar way, inspired by the integration of egocentric and allocentric information as found in the postrhinal cortex, the theory also predicts a new cell type, named geometry cell. Geometry cells encode the geometric layout of the local space relative to the environment center, independent of the animal's positions and headings within the local space. The predicted geometry cell provides pure allocentric high-level representations of local scenes to support the quick formation of cognitive map representations capturing the spatial layout of complex environments. The theory sheds new light on the neural mechanisms of spatial cognition and brain-inspired autonomous intelligent systems.

1. Introduction

Spatial cognition is one fundamental function of an animal to achieve long-term autonomy in the environment. It has been suggested that a map representation of the external world subserves brain functions such as navigation and planning, as it encodes the structure of the external world as well as the relationships between entities in the world with a form invariant to the observations of these entities (Tolman, 1948; Behrens et al., 2018). Humans and animals are able to efficiently create compact and sparse mental representations of the spatial structure of the environment for navigation (Poulter et al., 2018; Peer et al., 2020). Cognitive map representations are embodied by spatial-responsive cells found in the entorhinal-hippocampal neural circuit (Rolls and Kesner, 2006; Poulter et al., 2018). The firing activities of place cells in the hippocampus of mammalian brains constitute sparse representations of self-location in the environment (O'Keefe and Dostrovsky, 1971; Rich et al., 2014). Head-direction cells (HD cells) fire maximally when the animal faces in their preferred directions with respect to a reference frame, but are not tuned to the animal's position (Taube et al., 1990).

Grid cells in the medial entorhinal cortex (MEC) each encode multiple locations that collectively express a hexagonal grid pattern across the whole explored environment (Hafting et al., 2005; Killian et al., 2012). Spatial view cells are activated by visual scenes and can anchor the neural representations in the entorhinal-hippocampal neural circuit to landmarks, and therefore could reduce the accumulation of errors during path integration (Rolls et al., 1997; Collett and Graham, 2004; Hardcastle et al., 2015; Rolls and Wirth, 2018). These functionally distinct cell types encode the cognitive map of the environment in an allocentric reference frame.

Cognitive map representations are shaped by environment boundaries. Firing fields of place cells were observed to stretch in response to changes to the wall (O'Keefe and Burgess, 1996). The parahippocampal place cells in humans are activated by images of scenes regardless of their contents (Epstein and Kanwisher, 1998; Ekstrom et al., 2003), which is considered to encode the spatial layout (Epstein et al., 2007). The grid firing patterns are fragmented and distorted due to changes of environmental geometry (Barry et al., 2007; Derdikman et al., 2009; Stensola et al., 2015; Krupic et al., 2015). The allocentric geometric

---

information of environmental boundaries is conveyed by various cell types (Grieves and Jeffery, 2017). The "boundary cell" shows different firing patterns, like boundary vector cells (BVCs) (Barry et al., 2006; Lever et al., 2009), border cells (Solstad et al., 2008), boundary-off cells (Stewart et al., 2014), and all-boundary cells, including "annulus" and "bulls-eye" cells (Weible et al., 2012; Jankowski et al., 2015). An egocentric spatial representation of environmental boundaries is found in the dorsomedial striatum (Hinman et al., 2019). In the lateral entorhinal cortex (LEC), some neurons show selectivity for the egocentric bearing of environmental boundaries, centers, or goals in the environment (Wang et al., 2018). Neurons in the posterior parietal cortex represent the egocentric cue direction and HD conjunctively (Wilber et al., 2014). Neurons in the postrhinal cortex (POR) encode the conjunction of center bearing (CB) and head direction, with a moderate linear firing rate tuning by the center distance (CD) of the animal either positively or negatively (LaChance et al., 2019), where egocentric information can be transformed into allocentric spatial maps. These cell types encode geometry information of important entities, such as boundaries, centers, and landmarks, of the environment, and constitute computational building blocks in transforming the egocentric information sensed by an animal to allocentric cognitive map representations (Byrne et al., 2007; Bicanski and Burgess, 2018; Rolls, 2020; Evensmoen et al., 2021).

Neurons in many brain regions show selectivity to the association of multiple features (Sargolini et al., 2006; Rigotti et al., 2013). The conjunctive encoding of features could be implemented by a network that maps low dimensional feature space to high dimensional neural activity space (Si et al., 2014; Barak and Romani, 2021). An intriguing question to ask is whether the flexible and heterogeneous representations of geometry features could be described in the same framework of conjunctive encoding. To this end, we propose a theory of geometry representations to holistically characterize the computational mechanism underlying various boundary-related cells. Similarly, inspired by the transformation from egocentric perception into allocentric spatial maps in the postrhinal cortex, the theory predicts a new cell type named geometry cells, which encode the geometric layout of the local space relative to the center independent of the animal's positions and headings. The predicted geometry cells support the high-level spatial maps. The theory computationally explains the transformation from egocentric geometric sensory inputs to topological cognitive map representations that captures the spatial layout of complex environments. The theory describes the computational mechanism of various boundary-related cells (including the newly predicted geometry cells), which embody efficient spatial navigation at the neuronal level.

It is worthwhile to note that the understanding of the cognitive map system mainly attends to the representation of the entities of space with respect to the animals themselves. A pure allocentric neural coding of the space, i.e. encoding the relationship between entities, has not yet been found. This kind of pure allocentric representation is not dependent on the pose of the animal, but encodes the layout of the environment itself, and therefore could support abstract reasoning and planning in the view of an ideal observer. Inspired by the transformation from egocentric perception into allocentric spatial maps in the postrhinal cortex, we generalize the theory and predict that a new cell type, named geometry cells, could possibly exist to encode the geometric layout of the local space relative to the center, independent of the animal's positions and headings.

2. Results

To better understand the computations performed by various boundary-encoding cells, we formulate a computational framework that puts different cell types as building blocks into the transformation from egocentric representations of geometric information to allocentric neural codes of spatial layout. First, boundary features relative to self-location are tracked in high dimensional neural activity spaces by

boundary cells (Fig. 1). Second, the self-location relative to the environment center is conveyed in the activities of center-bearing cells in the postrhinal cortex (Fig. 2). These two sources of information are combined, possibly in the postrhinal cortex, resulting in a new cell type called geometry cell encoding boundary features relative to the environment center (Fig. 3). Geometry cells are selective to the conjunctions of the orientations and distances of boundaries from the viewpoint of the environment center, and therefore provide pure allocentric representations of the environment itself (Fig. 4).

2.1. Neural framework of conjunctive boundary representations

In this framework, boundary units are hypothetically arranged on a two-dimensional neuronal sheet (Fig. S1a). Each unit in the model is labeled by its coordinate (θ, r) on the neuronal sheet. The coordinate of a boundary unit encodes the conjunction of the bearing and the distance of a boundary. $\theta \in [0, 2\pi)$ encodes the direction in which the unit senses the boundary either in an egocentric or allocentric reference frame (Figs. S1b and 1 a). $r \in [0, \frac{\pi}{2})$ encodes the distance of the boundary relative to the center of the animal's head. The boundary distance is mapped nonlinearly to the distance dimension in the neuronal sheet, allowing the representation of wide distance coverage from vicinity to infinity (Fig. S1b) according to

$$r(\Theta) = arctan(\alpha d(\Theta)), \tag{1}$$

where $d(\Theta)$ is the distance of the boundary in direction Θ. The distance of the boundary could be estimated by the animal by depth perception. The boundaries outside of the visual field could be tracked by mechanisms similar to path integration, possibly implemented by attractor networks. $\alpha > 0$ is a parameter determining the steepness of distance mapping (Fig. S1c).

2.2. Egocentric boundary cell model

When the egocentric bearings of boundaries are mapped to the neuronal sheet, the framework gives rise to egocentric boundary cell model. Units in the egocentric boundary cell model account for the egocentric boundary cells found in the dorsomedial striatum (Hinman et al., 2019), the lateral entorhinal cortex (Wang et al., 2018), and the retrosplenial cortex (Alexander et al., 2020). Egocentric boundary units are driven by the geometric information of the boundaries within an egocentric reference frame. The firing rate $m(\theta, r)$ of the unit at the coordinate (θ, r) on the neuronal sheet is governed by the equation

$$m\left(\theta, r\right) = \int_0^{2\pi} \frac{exp\left[-(r - r(\Theta))^2 / 2\sigma_{dist}^2\right]}{\sqrt{2\pi\sigma_{dist}^2}}$$
$$\cdot \frac{exp\left[\kappa_{ang}cos\left(\theta - \Theta\right)\right]}{2\pi I_0\left(\kappa_{ang}\right)} d\Theta, \tag{2}$$

where $r(\Theta) \in [0, \frac{\pi}{2})$, given by Eq. (1), is the distance input at angle Θ in the physical environment. θ is the direction of a boundary in the egocentric reference frame. The integration represents the dendritic integration of a unit. The strength of the interaction between units is modeled by the product of a Gaussian function and a von Mises function. $\sigma_{dist} > 0$ and $\kappa_{ang} > 0$ are constants which describe the interaction range between units in the distance and orientation dimensions, respectively. $I_0(\kappa_{ang})$ is the modified Bessel function of order 0.

To investigate the firing activity of the model units, a virtual animal is simulated to explore a virtual environment with walls (Ref. Section 4). Given the sensory inputs, a pattern of activity emerges as a result of the integration of the current from presynaptic units on the neuronal sheet (Eq. (2), Fig. 1b Left). Depending on the units' positions on the neuronal sheet, egocentric boundary units show selectivity to a border at a given egocentric direction and distance to the animal (Figs. 1b Middle and S2). The same unit does not express localized firing fields in the allocentric
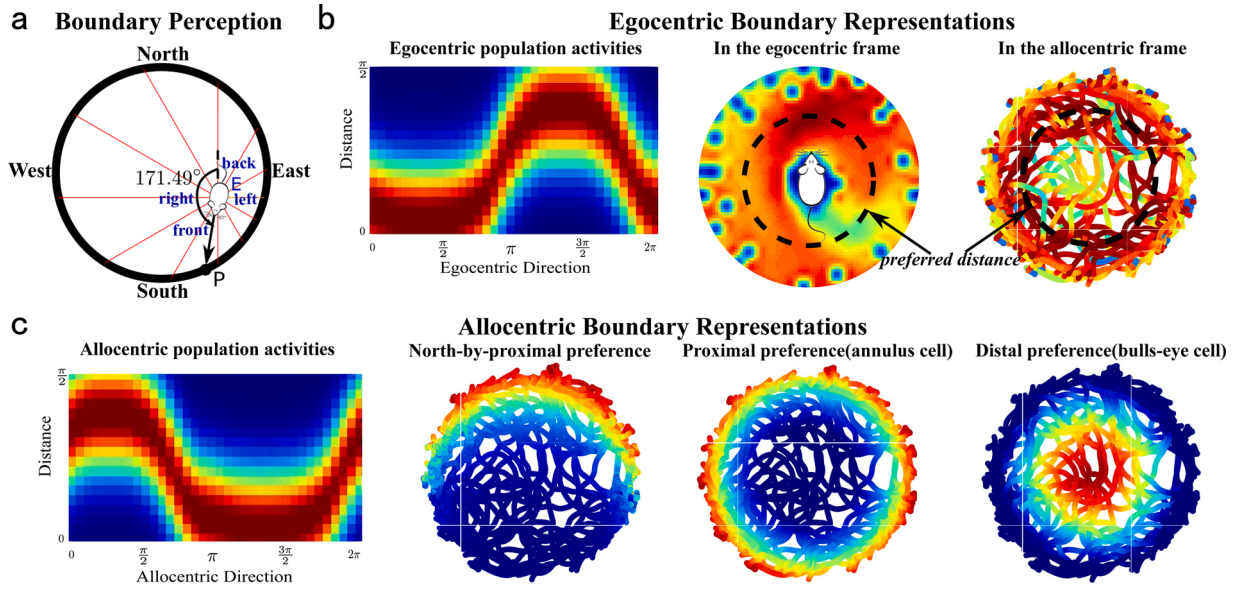
Fig. 1. Egocentric and allocentric representations of boundaries in the model. (**a**) **Boundary Perception.** The orientations and distances (red thin lines) of boundaries (black thick line) are perceived by the animal in an egocentric reference frame. (**b**) **Egocentric Boundary Representations. Left**: The population activity of egocentric boundary units encodes the distance of boundaries (*y*-axis) at each direction (*x*-axis) relative to the heading direction of the animal (Eq. (2)). The activity pattern corresponds to the perceived boundary distance and orientation in (**a**), and is color-coded from red to blue for high firing rate to zero firing rate. The left (0 to π) is closer to the boundary than the right (π to 2π). **Middle:** An egocentric boundary unit in the model that prefers boundaries at a certain distance to the front of the animal forms a field in the egocentric reference frame of the animal. **Right:** The egocentric boundary unit in (**Middle**) fires when the animal heads towards boundaries at a certain distance in an allocentric reference frame. The firing rate is color-coded on top of the trajectories. (**c**) **Allocentric Boundary Representations. Left**: The population activity of allocentric boundary units encodes the distance of boundaries (*y*-axis) at each direction (*x*-axis) in an allocentric reference frame with north as zero degrees (Eq. (3)). Note that the population activity of the allocentric boundary units is a 171.49° clockwise rotated version of the egocentric boundary cells shown in (**b Left**). The southeast is closer to the boundary than the northwest. **Firing rate maps from left to right**: An allocentric boundary unit in the model that prefers a proximal boundary at zero degrees fires at the north border; a pure boundary unit that prefers proximal boundaries has a firing field close to the border in a cylinder environment, similar to that of an annulus cell (Eq. (4)); the firing rate map of a pure boundary unit that prefers distal boundaries resembles that of a bulls-eye cell. (For interpretation of the references to color in this figure legend, the reader is referred to the web version of this article.)

reference frame, but its activation is contingent on the boundaries that appeared in a particular direction and distance relative to the trajectory (Figs. 1b Right and S3).

2.3. Allocentric boundary cell model

When the bearings of boundaries in an allocentric reference frame are mapped to the neuronal sheet, the framework gives rise to the allocentric boundary cell model. Allocentric boundary cell model explains the firing properties of the BVCs recorded in the subiculum (Lever et al., 2009; Stewart et al., 2014) and the border cells in the entorhinal cortex (Solstad et al., 2008). In the model, allocentric boundary units are arranged on a neuronal sheet with coordinate (θ, r). $\theta \in [0, 2\pi)$ encodes the allocentric direction of a boundary, i.e. relative to a reference frame in the environment. $r \in [0, \frac{\pi}{2})$ encodes the distance of the boundary relative to the center of the animal's head (Eq. (1)).

The firing rate $m(\theta, r)$ of a allocentric boundary unit is described as

$$m\left(\theta, r\right) = \int_0^{2\pi} \frac{exp\left[-(r - r(\Theta))^2/2\sigma_{dist}^2\right]}{\sqrt{2\pi\sigma_{dist}^2}} \cdot \frac{exp\left[\kappa_{ang}cos\left(\theta - \Theta + \Theta_{HD}\right)\right]}{2\pi I_0\left(\kappa_{ang}\right)} d\Theta,$$
(3)

where Θ_{HD} is the head direction of the animal. The model rotates the encoding of the boundaries in an egocentric reference frame by the amount Θ_{HD} into an allocentric reference frame. The rotation can be realized by a feedforward associative network receiving inputs from the HD cell network and the egocentric boundary cell network.

In a cylinder maze, some allocentric boundary units form firing fields at the border in particular directions, resembling those of the border cells found in MEC (Left in firing rate maps of Figs. 1c and S4d). Other

units fire along the wall with some distance away, and form fields similar to those of BVCs (Fig. S4a).

2.4. Pure boundary cell model

By integrating the activities of allocentric boundary units along the direction dimension θ, the allocentric boundary cell model generates pure boundary cell model. The firing rate $m(r)$ of a pure boundary unit at coordinate r is given by

$$m\left(r\right) = \int_0^{2\pi} \int_0^{2\pi} \frac{exp\left[-(r - r(\Theta))^2/2\sigma_{dist}^2\right]}{\sqrt{2\pi\sigma_{dist}^2}}$$
$$\cdot \frac{exp\left[\kappa_{ang}cos\left(\theta - \Theta + \Theta_{HD}\right)\right]}{2\pi I_0\left(\kappa_{ang}\right)} d\Theta d\theta.$$
(4)

Pure boundary unit at coordinate r encodes the boundaries at its preferred distance regardless of directions. As a result, pure boundary units are selective to certain distances of the boundaries but not to directions. The firing field of a pure boundary unit is typically paved along the boundary with preferred distance, and does not differentiate the direction of the boundary (Fig. S4c). In a cylinder environment, some pure boundary units express firing fields in the center or around the periphery of the maze (middle and right firing rate maps in Fig. 1c), similar to bulls-eye cells or annulus cells observed experimentally (Barry et al., 2006; Lever et al., 2009). Other pure boundary cells are most active when the animal is of medium distance away from the boundary (Fig. S4c). Pure boundary units reproduced the firing activities of the boundary cells recorded in the anterior claustrum, the rostral thalamus (Jankowski et al., 2015), the MEC (Solstad et al., 2008), and the anterior cingulate cortex (Weible et al., 2012).

a

Egocentric and Allocentric Transformation
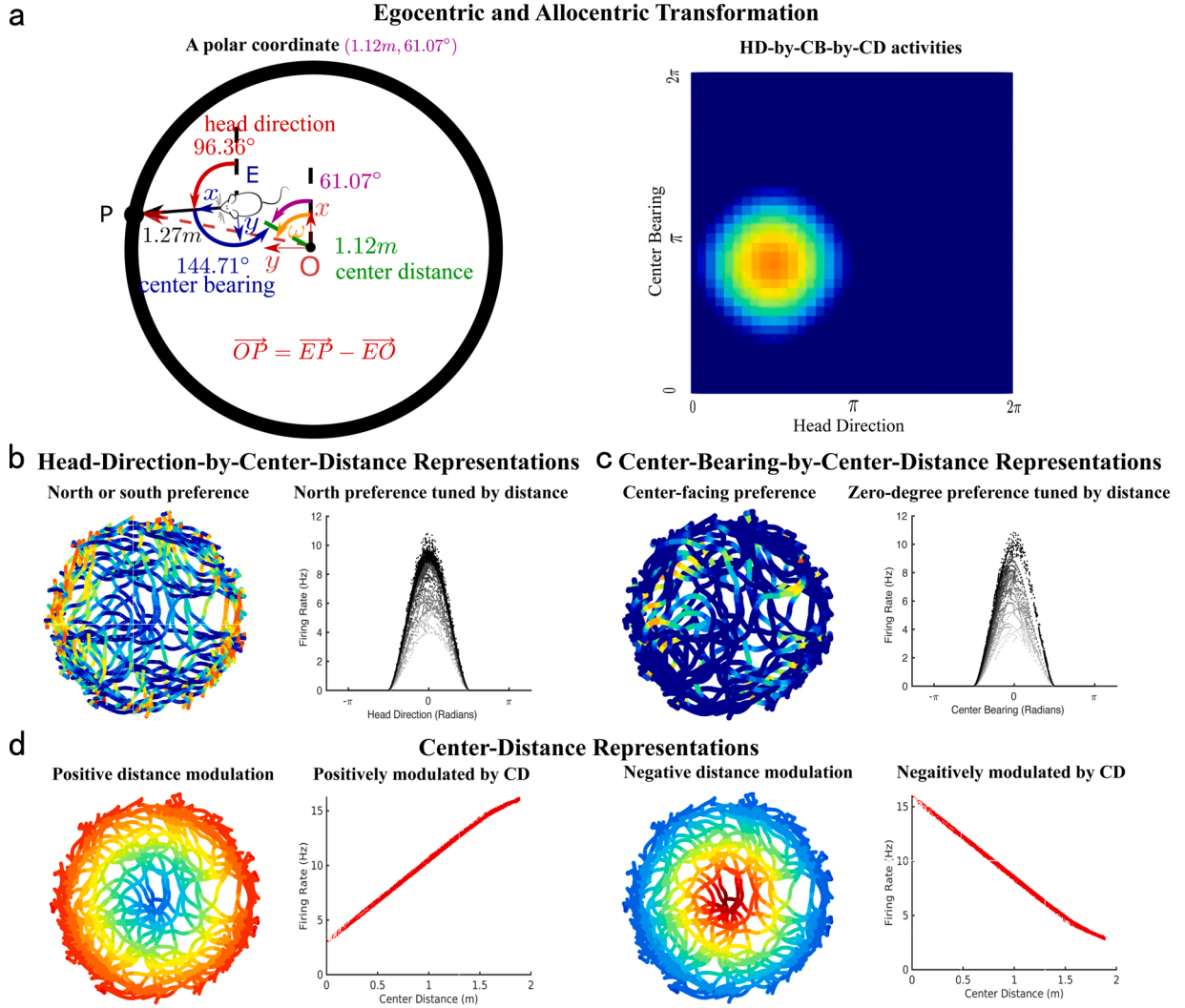
Fig. 2. Conjunctive representations of center bearing and head direction in the model. (**a**) **Egocentric and Allocentric Transformation. Left**: A schematic showing the head direction in an allocentric reference frame *O* and the center bearing as well as center distance in an egocentric reference frame *E*. The allocentric reference frame *O* is anchored to the north as zero degrees. The egocentric reference frame *E* takes the front direction as zero degrees. Point *P* in egocentric coordinate frame *E* can be transformed into coordinate frame *O* of the environment associated with the geometry representation. The boundary vector $\overrightarrow{OP}$ is indexed by its orientation ω. A polar coordinate (1.12m, 61.07°) is equivalently represented by HD (96.36°), CB (144.71°), and CD (1.12m). **Right**: An activity bump in the network of conjunctive center-bearing units encodes the conjunction of HD, CB, and CD (Eq. (5)), corresponding to the configuration of the animal shown in (**Left**). The center of the activity bump encodes the conjunction of the head direction (*x*-axis) and the center bearing (*y*-axis). The height of the activity bump is modulated positively by the center distance. (**b**) **Head-Direction-by-Center-Distance Representations. Left**: The sum of the firing rate maps of two HD-by-CD units in the model with north or south preference are positively modulated by CD. The two units fire along the trajectories heading towards north or south. Due to the positive modulation of CD, the firing rate of the units is higher when the animal is close to the border and lower when near the center. **Right**: The firing rate of a north-preferring HD-by-CD unit is peaked at its preferred HD (zero degrees). The HD tuning of the firing rate is variable due to modulation by CD. Gray colors from dark to light encodes large to the small CD. (**c**) **Center-Bearing-by-Center-Distance Representations. Left**: A CB-by-CD unit with center-facing preference and positive distance modulation fires only when toward the center. Due to the positive modulation of CD, the firing rate of this unit is higher when the animal is close to the border and lower when near the center. **Right**: The unit shown in (**left**) has a peak firing rate at its preferred CB, i.e. zero degrees. The CB tuning of the firing rate is variable due to the modulation by CD. CD is coded by black for large distances and light gray for small distances. (**d**) **Center-Distance Representations. Left**: The firing rate map of a center-distance unit with positive distance tuning shows an increased firing rate trend away from the geometric center. **Middle left**: The firing rates of the unit in (**left**) correlate positively with the center-distance. **Middle right**: The firing rate map of a center-distance unit with negative distance tuning shows a decreased firing rate trend away from the geometric center. (**Right**:) The firing rate of the unit in (**middle right**) negatively correlates with center-distance.

2.5. Conjunctive center-bearing cell model

The center-bearing in the egocentric coordinate and the HD of the animal could also be mapped onto the neuronal sheet. With additional center-distance modulation, the framework gives rise to a conjunctive center-bearing cell model for the space-responsive cells found in the POR (LaChance et al., 2019), which integrates egocentric and allocentric spatial information relative to the geometric center of the local environment. The self-location of the animal is represented by the vector $\overrightarrow{EO}$

relative to the geometric center of the local space (Fig. 2a left, Ref. Section 4). Since the angle of the animal in the polar coordinate system anchored to the center can be uniquely determined from the head direction and the center bearing, the space-responsive cells found in the POR encode the polar coordinate of the animal (Fig. 2a left).

The conjunctive center bearing units are organized on a two-dimensional neuronal sheet. Each conjunctive center bearing unit is labeled by its coordinate (θ_{hd}, θ_{cb}) on the neuronal sheet. θ_{hd} is the unit's preferred HD of the animal, and θ_{cb} the preferred center-bearing in the
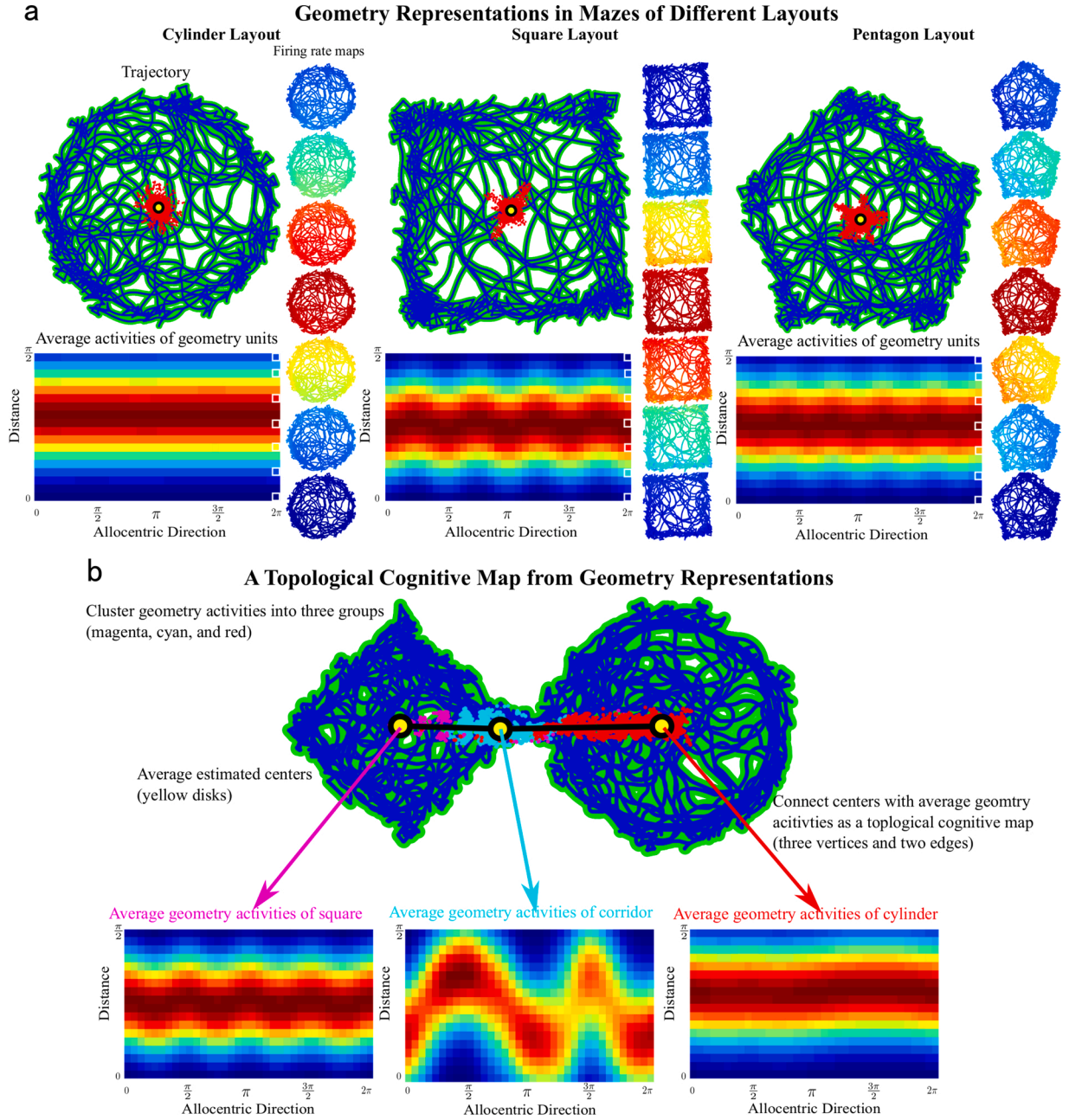
Fig. 3. Geometry units encode spatial layouts of local space. (**a**) **Geometry Representations in Mazes of Different Layouts.** Activities of geometry units (Eq. 7) in convex environments is able to differentiate open field mazes, such as a cylinder (**Left**), square (**Middle**), and pentagon (**Right**). In each subfigure, the virtual animal's trajectory (blue lines), estimated centers (red dots), and the average of the estimated centers (yellow disks) are shown on the top left. The average population activities of geometry units encode the conjunction of boundary distance and orientation relative to an allocentric reference frame anchored to the estimated center of the environment (bottom left). Since the boundaries are perceived without any occlusion, the activity pattern of geometry units is independent of the positions of the animal. The magnitudes of the constant firing rate maps of geometry units differ, however, due to their preferences for distance and HD (firing rate maps on the right, corresponding to seven units marked by seven white boxes in the bottom left). (**b**) **A Topological Cognitive Map from Geometry Representations.** A virtual animal explores a concave environment with two convex mazes connected by a narrow corridor (**top**). The estimated centers are distributed around three clusters (**top**, magenta, cyan, and red respectively). The average population activities of the three clusters differ from each other (**bottom**), and allow the distinction of the differences in the layout of the local space. The three connected cluster centers can be considered as a simple topological cognitive map. (For interpretation of the references to color in this figure legend, the reader is referred to the web version of this article.)

egocentric coordinate (Fig. 2a left). The firing activity of a center-bearing unit $(\theta_{hd}, \theta_{cb})$ is tuned conjunctively to head direction and center-bearing with a moderate linear modulation by center-distance (Fig. 2a right)

$$m(\theta_{hd}, \theta_{cb}, d) = kd[cos(\theta_{hd} - \Theta_{hd}) + cos(\theta_{cd} - \Theta_{cd}) - C_{inh}]_+ + b, \quad (5)$$

where C_{inh} is a uniform inhibition, and $[x]_+ = 0$ for $x < 0$, $[x]_+ = x$ for

$x \geq 0$. Θ_{cb} and d are the bearing and length of the vector $\overrightarrow{EO}$ respectively (Fig. 2a). k defines the steepness of the distance tuning. b is the baseline activity.

Integrating the population of the conjunctive center bearing units along different dimensions of the neuronal sheet gives rise to three other cell populations that encode HD-by-CD, CB-by-CD, and pure CD respectively. The HD-by-CD units are active when the animal points its
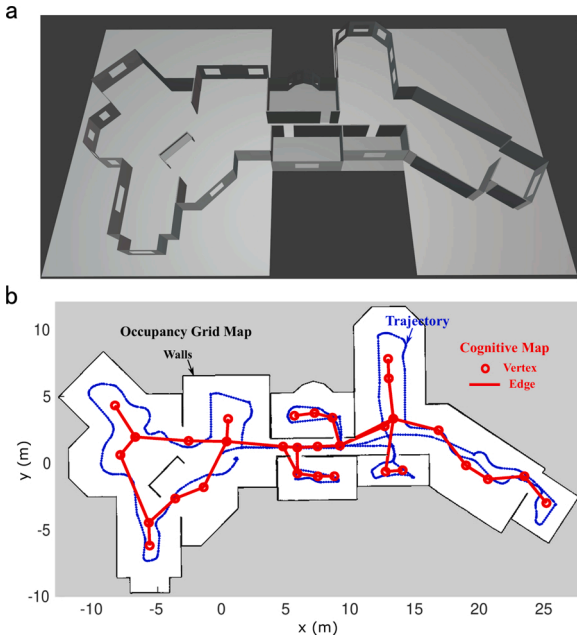
Fig. 4. The cognitive map generated from the theory of geometry representations of space. (**a**) **The virtual office environment.** A robot explores a $41m \times 22m$ virtual office environment with six rooms of different size. (**b**) **The topological cognitive map.** The trajectory (shown as a dotted blue line) of the robot has 1491 sample points. Using the neural representation of geometry cells, the spatial layout of the virtual office is described by a topological cognitive map with only 31 vertices (red dots) and 33 edges (red lines). Each vertex in the cognitive map is associated with a geometry representation. If the distance between two centers of geometry representations exceeds a certain dynamic threshold, a new vertex would be created. The black lines and gray areas describe an occupancy grid map, which is the estimated probability of a place being occupied by boundaries. (For interpretation of the references to color in this figure legend, the reader is referred to the web version of this article.)

head to the preferred HDs of the units (Fig. 2b left). The HD tuning curves of HD-by-CD units are modulated by the distance of the animal's body from the center, leading to high firing rate variability along with their preferred HDs (Fig. 2b right). In a similar fashion, the CB-by-CD units are tuned to CB, and the modulation by CD increases the irregularity of firing (Fig. 2c). The pure CD units show broad firing fields either on the border or around the center, depending on whether the firing rate tuning of CD is positive or negative (Fig. 2d).

2.6. Geometry cell model

Boundary cells (Fig. 1) encode boundary vectors $\overrightarrow{EP}$ (Fig. 2a) relative to the animal's self-position. The conjunctive center-bearing cell model describes the receptive fields of space-responsive cells found in the POR, and provides a representation of the vector $\overrightarrow{EO}$ pointing from the animal's self-position to the geometric center. The difference of these two vectors defines the boundary vector $\overrightarrow{OP}$ relative to the geometric center

$$\overrightarrow{OP} = \overrightarrow{EP} - \overrightarrow{EO}. \tag{6}$$

The vector $\overrightarrow{OP}$ could be embodied by a new cell type, named geometry cell. The hypothetical geometry cells map the conjunction of boundary distances and boundary directions relative to the environment center to a neuronal sheet. Each geometry unit in the model is labeled by its coordinate (θ, r) on the neuronal sheet. θ is the preferred allocentric direction and r is the preferred distance of the boundary. The firing rate of a geometry unit at (θ, r) is given by

$$m\left(\theta, r\right) = \int_0^{2\pi} \frac{exp\left[-(r - r(\omega))^2 / 2\sigma_{\mathrm{dist}}^2\right]}{\sqrt{2\pi\sigma_{\mathrm{dist}}^2}} \cdot \frac{exp\left[\kappa_{\mathrm{ang}} cos\left(\theta - \omega + \Theta_{\mathrm{HD}}\right)\right]}{2\pi I_0\left(\kappa_{\mathrm{ang}}\right)} d\omega, \tag{7}$$

where ω and $r(\omega)$ are the orientation and length of the vector $\overrightarrow{OP}$ respectively (Fig. 2a). Θ_{HD}, the head direction of the animal, describes the rotation from the allocentric reference frame to the egocentric reference frame.

The population activity of geometry cells characterizes the geometry of local space. In a cylinder maze, the population activity of geometry units forms a stripe firing pattern centered in neurons with a preferred distance equal to the radius of the maze (Fig. 3a left, Supplementary movie 1, Figs. S5–S6). The stripe firing pattern is an encoding of the center with a constant distance to the perimeter of the maze. The single-cell firing rate map of a geometry unit is uniform across the maze (Fig. 3a left). Different geometry units fire with different rates, depending on their preferred distances and HDs. Although geometry units do not have localized firing fields in the open field cylinder environment, they collectively encode the layout of local space. In convex mazes of different shapes, the population activities of geometry units keep persistent firing patterns reflecting layouts of the mazes (Fig. 3a middle and right, Supplementary movie 2–3). The neural activity of geometry units changes substantially at the conjunctions of compartments where the geometric layout of local space undergoes an abrupt transition (Fig. 3b, Supplementary movie 4). This kind of change in neural activity could support the topological representation of the environment that is composed of multiple subregions of a different shape.

2.7. Compact topological cognitive map capturing spatial layout

To further test the theory of geometry representations of space in a more realistic environment, a topological cognitive map is generated for a $41m \times 22m$ virtual office environment with six different sized rooms based on the models derived from the proposed theory (Fig. 4a, Supplementary movie 5).

Computed from the activities of boundary units and the conjunctive center-bearing units, the activity pattern of geometry units encodes the layout of the local space in relation to the center. Geometry units thus provide a high-level mapping of the local space invariant to the positions, orientations, and trajectories of the agent. Using the activity pattern of geometry units as a geometry representation of the entire local space, a topological map of the environment is constructed online quickly (Fig. 4b). While the agent explores the environment, a new vertex is added to the map once the distance between the centers of two local spaces exceeds a certain dynamic threshold. Connecting the centers associated with the geometry representations naturally results in a graph of the environment. The graph is composed of vertices that represent the center of a local space and edges that represent the estimated vectors between the connected vertices. The topological map (31 red vertices and 33 red edges in Fig. 4b) thus obtained is independent of the actual trajectories (blue lines in Fig. 4b) of the agent, since the map characterizes local geometry. Each room of the virtual office is represented by only 5 vertices on average. The topological cognitive map is compact and sparse, since the number of vertices is far less than the 1491 sample points of the robot trajectory.

3. Discussion

We have formulated a theory of conjunctive encoding for geometry representations of space. The hallmark of this theory is the conjunctive encoding of multiple behavior-relevant features on an abstract neuronal sheet. By mapping different inputs to the neuronal sheet, the network could flexibly encode multiple sources of information, and accounts for

various cell types found in different brain regions encoding geometry information of the environment (see Fig. 5a for a summary wiring diagram). The boundary cells (Fig. 1) conjunctively encode the head directions and the distances of boundaries relative to the animal's self-position, describing the vectors $\overrightarrow{EP}$ (Fig. 2a). The space-responsive cells found in the POR conjunctively encode the head direction, center bearing, and center distance, describing the animal's self-position relative to the center of local space (vector $\overrightarrow{EO}$ in Fig. 2a). To complete the relationships between the boundaries, self-position and the center of the local space, the theory predicts a new cell type, the geometry cells, as an embodiment of the vector $\overrightarrow{OP}$ (Fig. 2a). The geometry cells encode the conjunction of the orientations and the distances of boundaries relative to the geometric center of local space. The geometric features encoded by the geometry cells could be computed from the activities of boundary cells and conjunctive center-bearing cells (Eq. (6)), and could be implemented by neural network models (Wilber et al., 2014). Since the geometric features encoded by the geometry cells are invariant to the position of the animal in the local space, the geometry cells provide an allocentric encoding of the layout of the local space. Geometry cells furnish high-level representations of space and therefore support quick formation of spatial maps. The boundary cells, the conjunctive center bearing cells, and the geometry cells thus constitute a hierarchy of computations that extract high-level representations from the low-level perceptual information (Fig. S6). From the view of this theory, these cell types can be implemented by the same type of network architecture. It would be easier to develop brain regions containing these cell types using neural network motifs of the same structure. By routing different afferent inputs into the same network motif, cells develop rich neural codes of various spatial variables.

3.1. Relations to experiments

The theory gives rise to several models in a unified framework. The egocentric boundary cell model encodes the distance and orientation of the boundaries relative to the animal in an egocentric reference frame, and replicates the receptive fields of boundary-encoding cells found in

the dorsomedial striatum (Hinman et al., 2019), LEC (Wang et al., 2018), and retrosplenial cortex (Alexander et al., 2020). The allocentric boundary cell model encodes the boundaries at preferred distances to the animal and the preferred orientations with respect to an allocentric reference frame. Allocentric boundary units express similar firing fields as those of BVCs in the subiculum (Barry et al., 2006; Lever et al., 2009; Stewart et al., 2014) and border cells in MEC (Savelli et al., 2008; Solstad et al., 2008; Bjerknes et al., 2014). Units of the pure boundary cell model respond to the boundaries at particular distances regardless of their orientations, and show firing fields resembling those of annulus cells (Jankowski et al., 2015; Jankowski and O'Mara, 2015) and boundary-off cells/bulls-eye cells (Stewart et al., 2014; Weible et al., 2012; Solstad et al., 2008). Units of the conjunctive center-bearing cell model conjunctively encode three variables, namely allocentric head-direction, egocentric center-bearing, and center-distance. This model explains the firing patterns of many POR cells observed experimentally (LaChance et al., 2019). Some other POR cells are selective to two variables (LaChance et al., 2019), which can be modeled by dimension reduction of the conjunctive center-bearing cell model integrating along the unrelated dimension.

The proposed framework could also account for neurons that are selective to the vectors to objects, landmarks, or particular positions, such as goal locations (Høydal et al., 2019; Deshmukh and Knierim, 2013; Sarel et al., 2017). Recent evidence in humans has shown that the medial temporal lobe could encode self-centered bearings and distances toward reference points (Kunz et al., 2021). The distance and orientation of reference points, e.g. objects or landmarks, are mapped to the network, and tracked by recurrent mechanisms driven by self-motion.

The population activity of the geometry cell model represents the spatial layouts of the local space surrounding the animal. In the same spatial layout, each unit expresses uniform firing maps invariant to the positions in the environment (Fig. 3a). On the change of spatial layout, as the animal traverses in a heterogeneous environment, the activity of the geometry cells evolves into a different state (Fig. 3b). Thus, the geometry cells provide a computationally efficient encoding of the underlying structure of the local space, and map local space in disparate
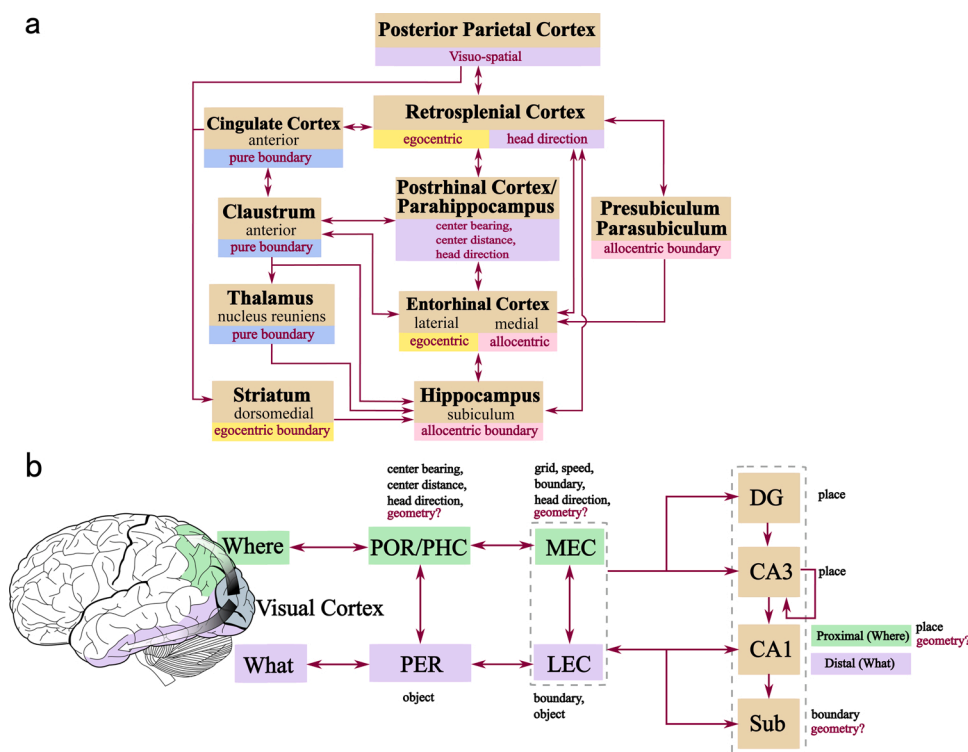
Fig. 5. The unified theory of geometry representations provides a coherent coding mechanism underlying various boundary-related cell types in the brain. (**a**) **A partial summary wiring diagram of major boundary-related regions found in the brain.** These boundary-related cells are example cell types explained by the unified theory of geometry representations. Pure boundary cells are found in the anterior claustrum, anterior cingulate cortex, and nucleus reuniens. Egocentric boundary cells are found in the dorsomedial striatum, LEC, and retrosplenial cortex. Allocentric boundary cells are found in the subiculum, MEC, presubiculum, and parasubiculum. The conjunctive center-bearing cells conjunctively encoding head direction, center-bearing, and center-distance are found in the postrhinal cortex. (**b**) **Where are the geometry cells?** The geometry cells are very likely to be found in the dorsal stream ("where pathway") of the two-streams hypothesis, supporting spatial geometry cognition together with boundary-related cells. The predicted brain areas where geometry cells may exist are POR, MEC, CA1, and subiculum in the hippocampus.

environments into efficient topological map representations based on environmental boundaries. The geometry cells could serve as a foundation for cognitive maps observed in the entorhinal-hippocampal neural circuit.

Our model assumes that all distances could be represented in the neuronal sheet. Recordings of boundary-responsive cells in large environments other than laboratory mazes of typical sizes should be carried out to test this assumption. Previous experiments in box mazes of side less than one meter have shown that sharper receptive fields of BVCs are distributed near boundaries (Lever et al., 2009). This inhomogeneous receptive field size could be either due to coarser resolution in the encoding of large distance, or due to less accurate update from sensory inputs of distal boundaries.

The proposed theory of geometry representations could be a general mechanism across species. In humans, cells in the medial temporal lobe are found to encode egocentric bearings toward reference points positioned throughout the environment. Some of these egocentric bearing cells also encode distance in conjunction with self-centered bearing (Kunz et al., 2021). By appropriate transformation, these egocentric bearing cells may give rise to spatial view cells, as found in the hippocampus of primates (Rolls, 1999, 2020). The egocentric bearing cells in humans might provide similar functions as the bearing encoding cells found in the POR and LEC of rodents. The proposed theory requires the input from HD cells, which are supposed to be provided by separate circuits. The boundary features in the egocentric reference frame and allocentric reference frame are encoded by egocentric boundary cells and allocentric boundary cells respectively. Then the self-location toward reference points, such as centers or objects, is represented in a polar coordinate system by cells in POR of rodents or in parahippocampal cortex (PHC) of primates. Combing the boundary information from the boundary-encoding cells and the self-location information in POR/PHC leads to a pure allocentric representation of the geometric layout of the local space, invariant to the positions and headings of the animal. This pure allocentric encoding of local space is embodied by the putative geometry cells. As demonstrated by the simulations in this study, the activities of geometry cells provide allocentric geometry encoding of local space, and could be further binded in place cells, with other inputs from grid cells, boundary vector cells and cells encoding semantic or reward information, through Hebbian-like competitive learning mechanisms resulting in object-level representations in the hippocampus. Grid cells integrate motion information as well as other afferent inputs from geometry cells, boundary vector cells and border cells, providing multi-resolutional allocentric representation of self-location in a global allocentric frame.

3.2. Predictions of the theory

The theory for geometry representations of space predicts that there exists a spectrum of boundary cells with various preferred distances. For example, some pure boundary cells would express circular-ring shaped firing fields in cylinder mazes (Fig. S4c). Circular-ring fields are intermediate firing patterns between those of annulus cells and bulls-eye cells. Experimental results have shown that some cells in MEC express fields along the wall but at some distance from the wall (Solstad et al., 2008), a prediction of the boundary vector cell model. Similar to the pure boundary cells, the egocentric boundary cells would have a family of cells that respond to boundaries in all egocentric directions (Hinman et al., 2019).

The geometry cells express uniform firing activity in convex environments. The firing rate of a geometry cell is dependent on the size and layout of the environment, and would show variations across different environments. In concave environments, e.g. mazes with the shape of a concave polygon or mazes with internal walls or objects, the firing map of a geometry cell would show some spatial tuning in the maze. The firing map of a geometry cell would not depend on the visual features of the environment, such as colors, textures, and objects, but is tuned to the

structure of the environment. The firing map of a geometry cell may not be controlled by visual landmarks on the walls, but is tied to the overall layout of the maze. Different from place cells, which show probabilistic recruitment across environments, geometry cells would be active in all environments.

3.3. Formation of geometry representations

The distance of boundaries could be perceived by the binocular vision in the dorsal visual pathway (Harris et al., 2008). The environmental boundaries are initially represented egocentrically. The transformation from an egocentric boundary representation into an allocentric representation is required (O'Keefe, 1991; Byrne et al., 2007; Bicanski and Burgess, 2018; Knierim et al., 2014). The retrosplenial cortex could be a potential hub of coordinate transformation (Epstein, 2008; Alexander et al., 2020). The geometry cells are very likely to reside in POR, or brain areas closely connected with POR (see Fig. 5b for prediction of brain areas where the geometry cells may exist). Related pieces of evidence come from functional magnetic resonance imaging (fMRI) experiments showing that PHC, the primate homolog of the rodent POR, is involved in representing spatial layout or learning spatial configurations of objects (Epstein and Kanwisher, 1998; Epstein et al., 2007; Bohbot et al., 2015). Via the projection from POR to the hippocampus, the population activity of geometry cells could be afferent to the hippocampus, facilitating the remapping of place cells in different environments. The geometry cells and boundary cells collectively constitute neural correlates of geometry cognition to support navigation and episodic memory.

3.4. Complementary modules of navigation

Some POR spatial cells provide an encoding of the self-location in a polar coordinate system. Entorhinal grid cells and hippocampal place cells represent self-location in cartesian coordinate systems. These different encoding schemes suggest that mammalian brains have parallel streams of spatial information processing. The polar representation is useful for computing vectors, while the cartesian representations are suitable for encoding large-scale space by multi-resolutional codes. Between the polar representations and the cartesian representations of space, there may exist a transformation network, which could possibly be performed by the entorhinal cortex.

Self-location is encoded in parallel by LEC egocentrically and by MEC allocentrically. MEC is considered to be the hub for allocentric encoding of self-location in spatial navigation. Anatomical studies have shown that LEC is very similar to the MEC in terms of intrinsic connectivity patterns and physiological properties of the neurons (Canto et al., 2008). The LEC is very likely to perform path integration in the egocentric coordinate system. Through the connections between LEC and MEC, the egocentric path-integration system in LEC may improve the performance of the allocentric path-integration system in the MEC and back. The egocentric navigation circuits and allocentric navigation circuits may show asynchronous developmental phases (Bullens et al., 2010; Ruggiero et al., 2016).

3.5. Quick formation of efficient cognitive map representation

The theory supports compact and sparse cognitive map representations. It successfully constructs topological cognitive maps representing the spatial layout of simple environments and a complex virtual office instead of sampling from trajectories. This allows fast construction of a high-level topological map of the environment without the need of dense coverage of the environment by trajectories (Ball et al., 2013; Zeng et al., 2020), or offline extraction from existing maps (Blochliger et al., 2018; Oleynikova et al., 2018). The topological map contains only the centers of local spaces and their connections, and is computationally efficient for navigation. The activity pattern of geometry cells is

associated with each vertex to characterize the geometry of local space. Such geometry representations allow accurate detection of the revisit of explored places during loop closures.

To conclude, the proposed theory validated the functions of various boundary-related cell types in the formation of compact and sparse cognitive map representations through simulations. The theory provides not only a unifying framework to organize boundary-related regions in the brain, but also insights into the mental representations of the spatial layout of the world. It sheds new light on developing better intelligent brain-like autonomous systems capable of understanding the topology of the external world and achieving long-term navigation.

4. Methods

4.1. Boundary vector relative to the environment center

The environment center is of behavioral importance for the exploration of the environment (Benjamini et al., 2011). The boundary vector could be represented with respect to the environment center.

The environment center is estimated as the centroid of the region circumvented by the boundaries. The boundary vector $\overrightarrow{EP}$ is represented relative to the environment center as $\overrightarrow{OP}$ in the reference frame at the center of the environment O (Fig. 2a)

$$\overrightarrow{OP} = \overrightarrow{EP} - \overrightarrow{EO}. \tag{8}$$

To get $\overrightarrow{OP}$, the translation vector $\overrightarrow{EO}$ has to be estimated. Indexing the boundary vector $\overrightarrow{OP}$ by its orientation ω, the translation vector $\overrightarrow{EO}$ is estimated by minimizing the discrepancy of the central symmetry between boundary vectors

$$\overrightarrow{EO}^* = \underset{\overrightarrow{EO}}{argmin} \int_0^\pi \|\overrightarrow{OP}(\omega) + \overrightarrow{OP}(\omega^*)\| d\omega, \tag{9}$$

where $\|\cdot\|$ computes the length of a vector. $\overrightarrow{OP}(\omega^*)$ is the boundary vector whose direction is the most consistent with the opposite direction of $\overrightarrow{OP}(\omega)$

$$\omega^* = \underset{\omega'}{argmin} |\omega + \pi - \omega'|. \tag{10}$$

Here $|\cdot|$ computes the distance on a cirle. ω' denotes the direction of an arbitrary boundary vector.

By putting the solution of Eq. (9) into Eq. (8), the boundary vectors are transformed to be relative to the environment center.

4.2. Network simulation in virtual environments

A virtual animal is simulated to explore an environment. The animal is able to sense the distance to boundaries in all directions. The distance label r of the neuronal sheet is discretized into 36 bins and the direction label θ is discretized into 18 bins. This results in 648 units in the egocentric boundary cell network, the allocentric boundary cell network, the geometry cell network and 1296 units for each of the conjunctive center bearing cell networks with positive/negative distance tuning. After dimension reduction, there are 18 units in the pure boundary cell network. Table 1 summarizes the parameters used in the simulations. The diameter of the walled cylinder environment is 4 m, and the side of the walled square environment is also 4 m.

To validate the biological plausibility of the proposed theory, simulations of realistic environments were performed in Gazebo (http://www.gazebosim.org). A rodent-like mobile robot, turtlebot3 burger (size 138 mm × 178 mm × 192 mm, http://www.robotis.us/turtlebot-3-burger-us/) equipped with a distance sensor 2D LiDAR (360 Laser Distance Sensor LDS-01) and an inertial measurement unit (IMU), is simulated to explore randomly in virtual environments. The virtual

Table 1
Parameters used in the theory.

Variable	α	σ_{dist}	κ_{ang}	k	b	C_{inh}
Value	0.6	0.36	45.0	15.0	6.0	0.5

environments are customized using world modeling software Blender (https://www.blender.org), typically including cylinder and square environments with walls of 0.5 m in height.

More specifically, while the robot traverses the environment, it detects boundaries and forms the egocentric boundary representations using the egocentric boundary cell model. The robot senses its movements through the IMU sensor, which functions as the vestibular system of an animal. The angular velocity information from the IMU sensor is integrated using the extended Kalman filter (EKF) to get a head-direction estimation. This head-direction estimation is used as an initial value for the Iterative Closest Point algorithm (Besl and McKay, 1992), which further improves the head-direction estimation by matching two sets of points observed by the LiDAR at consecutive time steps. Allocentric boundary representations are formed by combining the egocentric boundary representations and head-direction representations through the allocentric boundary cell model. Based on the allocentric boundary representation, the center of the local space is estimated, and is used as a reference point to encode the pose of the robot by the conjunctive center-bearing cell model. From the perspective of the center, the layout of the local space is represented in the activities of geometry cells by the transformation from allocentric boundary representations and conjunctive center-bearing representations. For each local space, the center and the corresponding geometry representation are attached, as the characterizing features of the local space, to a vertex in the cognitive map. The recruitment of a new vertex to the cognitive map is determined by a simple pattern separation mechanism. The pattern separation process computes the distance between the features of local spaces. If the distance from the features of the current local space to the features of the previous local space is larger than a certain dynamic threshold, a new vertex is linked to the cognitive map. The dynamic threshold is decided by the size of the current local space. Following the method in (Zeng et al., 2020), the cognitive map is maintained as a topological map with vertices and edges. Connecting the centers associated with the geometry representations naturally results in a graph of the environment (Fig. 4).

The models are implemented using C++ language, running on the Robot Operating System (ROS, https://www.ros.org) melodic on Ubuntu 18.04 LTS (Bionic Beaver). Python scripts are used to visualize the live state of our simulation of the robot system (Fig. S5).

Authors' contribution

Taiping Zeng and Bailu Si: conceptualization of this study, methodology, software, writing. Jianfeng Feng: conceptualization of this study, methodology, writing.

Acknowledgements

Appendix A. Supplementary data

Supplementary data associated with this article can be found, in the online version, at https://doi.org/10.1016/j.pneurobio.2022.102228.

References

Alexander, A.S., Carstensen, L.C., Hinman, J.R., Raudies, F., Chapman, G., Hasselmo, M., 2020. Egocentric boundary vector tuning of the retrosplenial cortex. Sci. Adv. 6.

Ball, D., Heath, S., Wiles, J., Wyeth, G., Corke, P., Milford, M., 2013. Openratslam: an open source brain-based slam system. Auton. Robots 34, 149–176.

Barak, O., Romani, S., 2021. Mapping low-dimensional dynamics to high-dimensional neural activity: a derivation of the ring model from the neural engineering framework. Neural Comput. 33, 827–852.

Barry, C., Hayman, R., Burgess, N., Jeffery, K.J., 2007. Experience-dependent rescaling of entorhinal grids. Nat. Neurosci. 10, 682.

Barry, C., Lever, C., Hayman, R., Hartley, T., Burton, S., O'Keefe, J., Jeffery, K., Burgess, N., 2006. The boundary vector cell model of place cell firing and spatial memory. Rev. Neurosci. 17, 71–98.

Behrens, T.E., Muller, T.H., Whittington, J.C., Mark, S., Baram, A.B., Stachenfeld, K.L., Kurth-Nelson, Z., 2018. What is a cognitive map? Organizing knowledge for flexible behaviour. Neuron 100, 490–509.

Benjamini, Y., Fonio, E., Galili, T., Havkin, G.Z., Golani, I., 2011. Quantifying the buildup in extent and complexity of free exploration in mice. Proc. Natl. Acad. Sci. U.S.A. 108, 15580–15587.

Besl, P.J., McKay, N.D., 1992. Method for registration of 3-d shapes. In: Sensor Fusion IV: Control Paradigms and Data Structures. International Society for Optics and Photonics, pp. 586–606.

Bicanski, A., Burgess, N., 2018. A neural-level model of spatial memory and imagery. eLife 7, e33752.

Bjerknes, T.L., Moser, E.I., Moser, M.B., 2014. Representation of geometric borders in the developing rat. Neuron 82, 71–78.

Blochliger, F., Fehr, M., Dymczyk, M., Schneider, T., Siegwart, R., 2018. Topomap: topological mapping and navigation based on visual slam maps. 2018 IEEE International Conference on Robotics and Automation (ICRA) 1–9.

Bohbot, V.D., Allen, J.J.B., Dagher, A., Dumoulin, S.O., Evans, A.C., Petrides, M., Kalina, M., Stepankova, K., Nadel, L., 2015. Role of the parahippocampal cortex in memory for the configuration but not the identity of objects: converging evidence from patients with selective thermal lesions and fmri. Front. Human Neurosci. 9, 431.

Bullens, J., Iglói, K., Berthoz, A., Postma, A., Rondi-Reig, L., 2010. Developmental time course of the acquisition of sequential egocentric and allocentric navigation strategies. J. Exp. Child Psychol. 107, 337–350.

Byrne, P., Becker, S., Burgess, N., 2007. Remembering the past and imagining the future: a neural model of spatial memory and imagery. Psychol. Rev. 114, 340.

Canto, C.B., Wouterlood, F.G., Witter, M.P., 2008. What does anatomical organization of entorhinal cortex tell us? Neural Plast. 2008, 381243.

Collett, T.S., Graham, P., 2004. Animal navigation: path integration, visual landmarks and cognitive maps. Curr. Biol. 14, R475–R477.

Derdikman, D., Whitlock, J.R., Tsao, A., Fyhn, M., Hafting, T., Moser, M.B., Moser, E.I., 2009. Fragmentation of grid cell maps in a multicompartment environment. Nat. Neurosci. 12, 1325.

Deshmukh, S.S., Knierim, J.J., 2013. Influence of local objects on hippocampal representations: landmark vectors and memory. Hippocampus 23, 253–267.

Ekstrom, A.D., Kahana, M.J., Caplan, J.B., Fields, T.A., Isham, E.A., Newman, E.L., Fried, I., 2003. Cellular networks underlying human spatial navigation. Nature 425, 184–188.

Epstein, R., Kanwisher, N., 1998. A cortical representation of the local visual environment. Nature 392, 598.

Epstein, R.A., 2008. Parahippocampal and retrosplenial contributions to human spatial navigation. Trends Cogn. Sci. 12, 388–396.

Epstein, R.A., Parker, W.E., Feiler, A.M., 2007. Where am i now? distinct roles for parahippocampal and retrosplenial cortices in place recognition. J. Neurosci. 27, 6141–6149.

Evensmoen, H.R., Rimol, L.M., Winkler, A.M., Betzel, R., Hansen, T.I., Nili, H., Håberg, A., 2021. Allocentric representation in the human amygdala and ventral visual stream. Cell Rep. 34, 108658.

Grieves, R.M., Jeffery, K.J., 2017. The representation of space in the brain. Behav. Process. 135, 113–131.

Hafting, T., Fyhn, M., Molden, S., Moser, M.B., Moser, E.I., 2005. Microstructure of a spatial map in the entorhinal cortex. Nature 436, 801.

Hardcastle, K., Ganguli, S., Giocomo, L.M., 2015. Environmental boundaries as an error correction mechanism for grid cells. Neuron 86, 827–839.

Harris, J., Nefs, H., Grafton, C., 2008. Binocular vision and motion-in-depth. Spatial Vision 21, 531–547.

Hinman, J.R., Chapman, G.W., Hasselmo, M.E., 2019. Neuronal representation of environmental boundaries in egocentric coordinates. Nat. Commun. 10, 2772.

Høydal, O.A., Skytøen, E.R., Andersson, S.O., Moser, M.B., Moser, E.I., 2019. Object-vector coding in the medial entorhinal cortex. Nature 568, 400–404.

Jankowski, M.M., O'Mara, S.M., 2015. Dynamics of place, boundary and object encoding in rat anterior claustrum. Front. Behav. Neurosci. 9, 250.

Jankowski, M.M., Passecker, J., Islam, M.N., Vann, S., Erichsen, J.T., Aggleton, J.P., O'Mara, S.M., 2015. Evidence for spatially-responsive neurons in the rostral thalamus. Front. Behav. Neurosci. 9, 256.

Killian, N.J., Jutras, M.J., Buffalo, E.A., 2012. A map of visual space in the primate entorhinal cortex. Nature 491, 761–764.

Knierim, J.J., Neunuebel, J.P., Deshmukh, S.S., 2014. Functional correlates of the lateral and medial entorhinal cortex: objects, path integration and local-global reference frames. Philos. Trans. R. Soc. B: Biol. Sci. 369, 20130369.

Krupic, J., Bauza, M., Burton, S., Barry, C., O'Keefe, J., 2015. Grid cell symmetry is shaped by environmental geometry. Nature 518, 232.

Kunz, L., Brandt, A., Reinacher, P.C., Staresina, B.P., Reifenstein, E.T., Weidemann, C.T., Herweg, N.A., Patel, A., Tsitsiklis, M., Kempter, R., Kahana, M.J., Schulze-Bonhage, A., Jacobs, J., 2021. A neural code for egocentric spatial maps in the human medial temporal lobe. Neuron 109, 2781–2796 e10.

LaChance, P.A., Todd, T.P., Taube, J.S., 2019. A sense of space in postrhinal cortex. Science 365, eaax4192.

Lever, C., Burton, S., Jeewajee, A., O'Keefe, J., Burgess, N., 2009. Boundary vector cells in the subiculum of the hippocampal formation. J. Neurosci. 29, 9771–9777.

O'Keefe, J., 1991. An allocentric spatial model for the hippocampal cognitive map. Hippocampus 1, 230–235.

O'Keefe, J., Burgess, N., 1996. Geometric determinants of the place fields of hippocampal neurons. Nature 381, 425.

O'Keefe, J., Dostrovsky, J., 1971. The hippocampus as a spatial map: preliminary evidence from unit activity in the freely-moving rat. Brain Res. 341.

Oleynikova, H., Taylor, Z., Siegwart, R., Nieto, J., 2018. Sparse 3d topological graphs for micro-aerial vehicle planning. 2018 IEEE/RSJ International Conference on Intelligent Robots and Systems (IROS) 1–9.

Peer, M., Brunec, I.K., Newcombe, N.S., Epstein, R.A., 2020. Structuring knowledge with cognitive maps and cognitive graphs. Trends Cogn. Sci.

Poulter, S., Hartley, T., Lever, C., 2018. The neurobiology of mammalian navigation. Curr. Biol. 28, R1023–R1042.

Rich, P.D., Liaw, H.P., Lee, A.K., 2014. Large environments reveal the statistical structure governing hippocampal representations. Science 345, 814–817.

Rigotti, M., Barak, O., Warden, M.R., Wang, X.J., Daw, N.D., Miller, E.K., Fusi, S., 2013. The importance of mixed selectivity in complex cognitive tasks. Nature 497, 585–590.

Rolls, E., 1999. Spatial view cells and the representation of place in the primate hippocampus. Hippocampus 9, 467–480.

Rolls, E.T., 2020. Spatial coordinate transforms linking the allocentric hippocampal and egocentric parietal primate brain systems for memory, action in space, and navigation. Hippocampus 30, 332–353.

Rolls, E.T., Kesner, R.P., 2006. A computational theory of hippocampal function, and empirical tests of the theory. Prog. Neurobiol. 79, 1–48.

Rolls, E.T., Robertson, R.G., Georges-François, P., 1997. Spatial view cells in the primate hippocampus. Eur. J. Neurosci. 9, 1789–1794.

Rolls, E.T., Wirth, S., 2018. Spatial representations in the primate hippocampus, and their functions in memory and navigation. Prog. Neurobiol. 171, 90–113.

Ruggiero, G., D'Errico, O., Iachini, T., 2016. Development of egocentric and allocentric spatial representations from childhood to elderly age. Psychol. Res. 80, 259–272.

Sarel, A., Finkelstein, A., Las, L., Ulanovsky, N., 2017. Vectorial representation of spatial goals in the hippocampus of bats. Science 355, 176–180.

Sargolini, F., Fyhn, M., Hafting, T., McNaughton, B.L., Witter, M.P., Moser, M.B., Moser, E.I., 2006. Conjunctive representation of position, direction, and velocity in entorhinal cortex. Science 312, 758–762.

Savelli, F., Yoganarasimha, D., Knierim, J.J., 2008. Influence of boundary removal on the spatial representations of the medial entorhinal cortex. Hippocampus 18, 1270–1282.

Si, B., Romani, S., Tsodyks, M., 2014. Continuous attractor network model for conjunctive position-by-velocity tuning of grid cells. PLoS Comput. Biol. 10, e1003558.

Solstad, T., Boccara, C.N., Kropff, E., Moser, M.B., Moser, E.I., 2008. Representation of geometric borders in the entorhinal cortex. Science 322, 1865–1868.

Stensola, T., Stensola, H., Moser, M.B., Moser, E.I., 2015. Shearing-induced asymmetry in entorhinal grid cells. Nature 518, 207.

Stewart, S., Jeewajee, A., Wills, T.J., Burgess, N., Lever, C., 2014. Boundary coding in the rat subiculum. Philos. Trans. R. Soc. B: Biol. Sci. 369, 20120514.

Taube, J.S., Muller, R.U., Ranck, J.B., 1990. Head-direction cells recorded from the postsubiculum in freely moving rats. I. Description and quantitative analysis. J. Neurosci. 10, 420–435.

Tolman, E.C., 1948. Cognitive maps in rats and men. Psychol. Rev. 55, 189.

Wang, C., Chen, X., Lee, H., Deshmukh, S.S., Yoganarasimha, D., Savelli, F., Knierim, J.J., 2018. Egocentric coding of external items in the lateral entorhinal cortex. Science 362, 945–949.

Weible, A.P., Rowland, D.C., Monaghan, C.K., Wolfgang, N.T., Kentros, C.G., 2012. Neural correlates of long-term object memory in the mouse anterior cingulate cortex. J. Neurosci. 32, 5598–5608.

Wilber, A.A., Clark, B.J., Forster, T.C., Tatsuno, M., McNaughton, B.L., 2014. Interaction of egocentric and world-centered reference frames in the rat posterior parietal cortex. J. Neurosci. 34, 5431–5446.

Zeng, T., Tang, F., Ji, D., Si, B., 2020. Neurobayesslam: Neurobiologically inspired Bayesian integration of multisensory information for robot navigation. Neural Netw. 126, 21–35.